Geomechanics and Engineering, *Vol. 37, No. 1 (2024) 49-64*
https://doi.org/10.12989/gae.2024.37.1.049

Deep learning-based AI constitutive modeling for sandstone and mudstone under cyclic loading conditions

Luyuan Wu*[1], Meng Li[1a], Jianwei Zhang[1b], Zifa Wang[1,2], Xiaohui Yang[3] and Hanliang Bian[1]

[1]*School of Civil Engineering and Architecture, Henan University, Jinming road, Kaifeng, 475004, He nan, China*
[2]*CEAKJ ADPRHexa, Inc, Street, Shao guan, 512000, Guangdong, China*
[3]*Henan Provincial Engineering Research Center for Artificial Intelligence Theory and Algorithm, Henan University, Jinming road, Kaifeng, 475004, He nan, China*

(*Received October 13, 2023, Revised January 24, 2024, Accepted March 10, 2024*)

Abstract. Rocks undergoing repeated loading and unloading over an extended period, such as due to earthquakes, human excavation, and blasting, may result in the gradual accumulation of stress and deformation within the rock mass, eventually reaching an unstable state. In this study, a CNN-CCM is proposed to address the mechanical behavior. The structure and hyperparameters of CNN-CCM include Conv2D layers × 5; Max pooling2D layers × 4; Dense layers × 4; learning rate=0.001; Epoch=50; Batch size=64; Dropout=0.5. Training and validation data for deep learning include 71 rock samples and 122,152 data points. The AI Rock Constitutive Model learned by CNN-CCM can predict strain values(ε_1) using Mass (M), Axial stress (σ_1), Density (ρ), Cyclic number (N), Confining pressure (σ_3), and Young's modulus (E). Five evaluation indicators R^2, *MAPE*, *RMSE*, *MSE*, and *MAE* yield respective values of 0.929, 16.44%, 0.954, 0.913, and 0.542, illustrating good predictive performance and generalization ability of model. Finally, interpreting the AI Rock Constitutive Model using the SHAP explaining method reveals that feature importance follows the order $N > M > \sigma_1 > E > \rho > \sigma_3$.Positive SHAP values indicate positive effects on predicting strain ε_1 for N, M, σ_1, and σ_3, while negative SHAP values have negative effects. For E, a positive value has a negative effect on predicting strain ε_1, consistent with the influence patterns of conventional physical rock constitutive equations. The present study offers a novel approach to the investigation of the mechanical constitutive model of rocks under cyclic loading and unloading conditions.

Keywords: cyclic loading and unloading; deep Learning; rock constitutive model; rock triaxial compression tests; shap explaining

1. Introduction

Rocks are complex fractured geological media with numerous randomly distributed defects such as joints and cracks. These rocks are natural geological materials that possess inherent defects. The constitutive equation, as a mathematical model, plays an irreplaceable role in the development of rock mechanics theory and numerical simulation by representation of rock mechanical properties, through stres-strain relations (Zhou *et al*. 2019, Ahmed *et al.* 2020). Many researchers have studied the strength and deformation capacity of rocks under different loading conditions and developed various constitutive models that account for nonlinearity, anisotropy, rheology, elastoplasticity, and other rock properties, providing a solid theoretical foundation for engineering practice (Xu and Wei 2002, Zhou and Zhu 2010, Li *et al.* 2012, Sloan *et al*. 2013, Pourhosseini and Shabanimashcool 2014). However, rocks often undergo repeated cyclic loading and unloading in activities, such as earthquakes, rock blasting, coal mining, pressurized injection and extraction, tunnel excavation, and underground gas storage chambers. (Haimson 1978, Ray *et al.* 1999, Crotogino *et al*. 2001, Heap *et al.* 2010, Xiao *et al.* 2010, Zhang *et al.* 2023, Zhao *et al.* 2024). The process of cyclic loading and unloading in rocks results in a gradual accumulation of damage. Therefore, studying the deformation characteristics and mechanical property evolution of rocks under cyclic loading and unloading conditions can provide a better foundation for the rational design and protection of engineering structures.

Regarding the research on traditional constitutive models for rocks under cyclic loading and unloading, Mo 1988 conducted cyclic loading tests on sandstone and marble, and proposed an internal time-dependent constitutive equation for rocks based on irreversible thermodynamics and the concept of kimu of internal variables. However, the material functions in the model exhibit complexity, featuring numerous parameters without clear physical meanings. Wang *et al.* (2012) carried out triaxial cyclic loading tests on granite and proposed an internal variable fatigue constitutive model that can reflect the change of rock deformation modulus under cyclic loading conditions. However the model falls short in fully depicting the stress-strain relationship of rocks. In addition, under cyclic loading, rocks actually undergo a process of

*Corresponding author, Professor
E-mail: wulymp@henu.edu.cn
[a]Graduate student
E-mail: lm@henu.edu.cn
[b]Professor
E-mail: zjw@henu.edu.cn

ISSN: 2005-307X (Print), 2092-6219 (Online)

cumulative damage (Xie 1990), suggesting that the application of rock damage theory to the study of constitutive model is feasible. A variety of rock damage measurement methods are commonly used, including the elastic modulus method, maximum strain method, residual strain method, energy dissipation method, ultrasonic velocity method, and acoustic emission cumulative count method. Zhou *et al.* (2020) reviewed the statistical constitutive damage model and developed a new statistical damage model that considers failure mode transition by introducing the rock brittleness parameter-BI. Zhou *et al*. (2017) extended the damage constitutive model with weibull distribution and proposed a constitutive model for rocks subjected to cyclic stress-temperature conditions. Moradian *et al*. (2016) conducted uniaxial compression tests on granite prismatic specimens with pre-existing defects and monitored their cracking process through acoustic emission and high-speed video imaging, enabling the analysis of the characterization of the acoustic emission parameters and the evolution of the cracking sequence for each crack level are analyzed. The classification of crack levels according to micro- and macro-crack damage is presented. However, rock damage is influenced by both micro-defects within the material and the stress state of the rock micro-elements. The aforementioned models have certain limitations. The deformation and failure of rocks fundamentally encompass the process of internal energy dissipation and release of rocks, and energy dissipation is the internal dynamic of damage development (Xie *et al*. 2008), enabling a more profound exploration of the relationship between energy dissipation and damage evolution during rock failure processes. In order to further analyze the relationship between energy dissipation and damage evolution during the process of rock failure, many researchers have investigated studies on the nonlinear mechanical properties of rocks from an energy perspective and have yielded substantial insights. Zhou *et al.* (2019) established a link between the energy transformation law and the mechanical properties of rocks, and developed a constitutive model of rocks under triaxial compression. Liu *et al.* (2013); Tian and Yu (2014) investigated the energy dissipation characteristics of the rock loading deformation process by calculating the energy conversion at each stage of loading, Liu *et al*. (2011) derived damage evolution equations based on the principle of energy dissipation and established a constitutive model for rock damage. Nonetheless, rocks may simultaneously experience different deformation characteristics, including elastic, plastic, creep strain, loading and unloading, and microcracks. In order to effectively reveal these characteristics, there is an urgent to develop a constitutive model that can properly analyze these features.

In the field of rock mechanics, computer-based approaches have proven to effective in analyzing and proposing constitutive models for rock materials. One alternative to traditional constitutive modeling methods is the use of neural network algorithms, which have gained popularity in engineering. Ali *et al*. (2019) conducted a study where they trained an artificial neural network (ANN) with 80 neurons per hidden layer to account for variations in a single crystal under uniaxial tension or shear loads. However, it is worth noting that shallow ANNs have limitations when it comes to analyzing nonlinear relationships due to their simple architecture (Zhang *et al*. 2020). Recent studies have shown that deep learning, a form of artificial intelligence, holds great potential in the development of constitutive models for materials. Deep learning techniques such as back propagation neural network (BPNN), fully connected neural network (FCNN), gated recurrent unit (GRU), long short-term memory (LSTM), and recurrent neural network (RNN), and convolutional neural network (CNN)) can handle complex environmental information, unclear background knowledge, and fuzzy reasoning rules. The feature extraction capability of CNN is particularly advantageous compared to other neural networks. Wu *et al*. (2018) attempted to optimize the constitutive model of constrained recovery of shape memory alloys and developed a BPNN model to achieve this. Xu *et al*. (2023) constructed a Deep Neural Network (DNN) model with four hidden layers and 100 neurons in each layer to predict the complete residual stress–strain response of UHPC materials after high temperature. Wu *et al*. (2023) proposes a CNNCM machine learning method to describe the stress–strain relationship in the process of the rock failure.

In recent years, deep learning algorithms, such as convolutional neural networks (CNN), have shown great potential in developing constitutive models for materials. However, research on deep learning-based constitutive models for rocks under cyclic loading and unloading remains scarce or almost nonexistent. This study aims to fill this research gap by conducting triaxial compression tests on rock samples, with the extraction of experimental data on uniaxial and triaxial from journal papers and comparing deep learning algorithms including BPNN, DNN, and CNN, to proposed a CNN-CCM constitutive model for rock cyclic loading. The input features for the model include Stress, Young's modulus, density, confining pressure, mass, and cyclic number loading, and strain was designated as the output feature for multi-factor single-output analysis. The weight relationships for these parameters were obtained through training data. Furthermore, the trained weight model data underwent validation, leading to the selection of the optimal weight model to establish the constitutive model for rock cyclic loading and unloading. Finally, the generalization and feasibility of the model were analyzed,leading to the proposal of a constitutive model for rock cyclic loading .This model can be used to analyze the failure and deformation of the overall rock stress-strain process.

2. Methodology

2.1 Traditional cyclic loading constitutive model for rocks

In Table 1, various traditional constitutive models for cyclic loading and unloading are presented. These models show that the mechanical properties of rocks under cyclic loading conditions are more complex and diverse than those

Table 1 Traditional constitutive model of cyclic loading

Reference	Rock type	Method	Constitutive equation
Luo and Li (2020)	sandstone	weibull distribution	$F_0(\ln\frac{E\varepsilon_1}{\sigma_1-2\mu\sigma_3})^{\frac{1}{m}}=\frac{\sigma_1 E\varepsilon_1}{\sigma_1-2\mu\sigma_3}=F$
Jing *et al*. (2022)	coal rock	weibull distribution	$\frac{\sigma_1-2\mu\sigma_3}{E\varepsilon_1}=\exp\left(-(\frac{(\sigma_1-\sigma_3)E\varepsilon_1}{\sigma_1-2\mu\sigma_3 F_0})^m\right)$
Zhang *et al*. (2015)	sandstone	weibull distribution	$\sigma_1=E_0\varepsilon_1\exp[-(F/F_0)^m]+2\mu\sigma_3$
Gong *et al.* (2022)	Shale, red sandstone, and green sandstone	energy dissipation	$\sigma=K'(1-D)E\varepsilon=K'(1-\frac{cu^0}{U^p})E\varepsilon$
Liu *et al*. (2016)	Sandy mudstone	energy dissipation	$\sigma=\begin{cases}\frac{\varepsilon-\varepsilon^{pi-1}}{\varepsilon_{i-1}-\varepsilon p_{i-1}}K_i(1-D)^{mi-1}E\varepsilon & \varepsilon^{pi-1}<\varepsilon<\varepsilon_{i-1}\\ K_i(1-D)^{mi}E\varepsilon & \varepsilon\geq\varepsilon_{i-1}\end{cases}$
Tao and Mo (1990)	sandstone	Endochronic constitutive	$\{d\sigma\}=[D]\{d\varepsilon\}-\{dF\}$
Wang *et al.* (2013)	granite	Fatigue constitutive model with internal variables	$E=A(\overline{\sigma}^{cr})^n\varepsilon_{1r}^{\ m}$
Cerfontaine (2017)	marble,sandstone, and granite	Elastoplastic constitutive model	$\dot{s}=E(\dot{e}-\dot{e}^p)$
Liu *et al*. (2017)	Jointed rock	Discrete element based model	$\sigma=\begin{cases}\pi\times C_i\times(\frac{u_l}{u_i})^p, \dot{u}>0\\ \pi\times C_i\times(\frac{u_u}{u_i})^q, \dot{u}<0\\ \pi\times C_i\times(\frac{u_{rl}}{u_i})^r, \dot{u}>0\end{cases}$

under monotonic conditions. They exhibit significant hysteresis due to the repeated accumulation of plastic strain. Many researchers have derived different types of constitutive equations, including those based on elasto-plasticity, internal variables, discrete elements, energy dissipation, and weibull distribution. However, these models often have an excess of material and model parameters. Some model parameters lacking clear physical meanings or are numerous and meaningless obtained through curve fitting. Mutual validation and explicit parameters to control the size and shape of the hysteresis loop are lacking in some models, resulting in non-smooth transitions between loading. Furthermore, some constitutive equations are based on laboratory tests, which are only applicable to specific loading conditions, limiting their universal applicability. Influential factors such as the cyclic loading waveform, load parameters, and water saturation are often not considered in these models. Future research on constitutive modeling should focus on addressing these limitations and enhancing the understanding of rock behavior under cyclic loading and unloading conditions.

2.2 Data collection and preprocessing

As show in Fig. 1, an MTS 815 2.0 electro-hydraulic servo rock mechanics testing system was used for the experiments. Triaxial compression tests were carried out on sandstone specimens subjected to varying confining pressures. The rock samples were sourced from mining drilling in Chensilou coal mine, Yongcheng City, Henan Province, China. Standard-sized specimens, measuring 50 mm × 100 mm, were prepared for the triaxial compression tests. The rock samples used in this experiment are provided.

The data collected for this study consists of both experimental data and extracted data from papers and journals. The experimental data includes 10 sets of data, while the extracted data from papers and journals consist of 61 sets of data (Su and Yang 2006, Deng 2013, Yang *et al.* 2018, Zhou 2018, Zhang 2019, Zhou 2019, Gong *et al.* 2020, Meng *et al.* 2020, Chen *et al.* 2021, Liu *et al.* 2021, Sun 2022, Wang 2022, Jiang *et al.* 2023). In total, there are 71 sets of data with a total of 122,152 data points. The rocks included in the dataset are sandstone, red sandstone, limestone, green sandstone, black sandstone, yellow sandstone, mudstone, granite, shale, and marble. According to the literature and data availability, 6 input variables are considered, Mass(M), Axial stress (σ_1), Density(ρ),Cyclic number(N), Confining pressure(σ_3) and Young's modulus(E).the output variable of Neural Network models is the axial strain(ε_1). Among of the total 122152 data, 60% were randomly selected for training the predictive constitutive models, the 20% were used to validate the performance of the developed constitutive models, while the remaining 20% were used to test the performance of the developed constitutive models in predicting the strain based

Table 2 Statistics analysis of the training, validating and testing datasets

	Properties	Average	Standard deviation	Minimum	Median	Maximum
Training dataset (44)	Circle	9.010	5.546	1	8	32
	Mass	495.248	77.139	366.090	480.850	877.190
	Density	2.519	0.092	1.950	2.542	2.690
	Modulus	19.501	11.630	0.300	17.020	94.410
	Pressure	12.587	11.257	0	10	60
	Stress	36.806	43.680	43.680	26.680	391.985
	Strain	6.597	6.448	1.730E-05	5.146	56.410
Validating dataset (14)	Circle	7.857	4.574	1	7	18
	Mass	493.263	111.286	389.560	480.810	876.320
	Density	2.459	0.155	1.960	2.557	2.614
	Modulus	16.016	8.595	0.450	13.360	53.010
	Pressure	7.868	7.578	0	5	30
	Stress	23.972	20.734	0	17.496	111.249
	Strain	5.412	4.737	5.660E-4	4.549	56.230
Testing dataset (13)	Circle	9.119	4.756	1	9	21
	Mass	480.478	16.504	382.690	481.340	527.920
	Density	2.512	0.079	1.950	2.510	2.690
	Modulus	19.628	9.909	1.040	17.040	62.080
	Pressure	9.435	7.888	0	5	40
	Stress	38.401	43.249	0.032	27.171	345.680
	Strain	5.740	4.651	6.642E-4	4.826	48.520

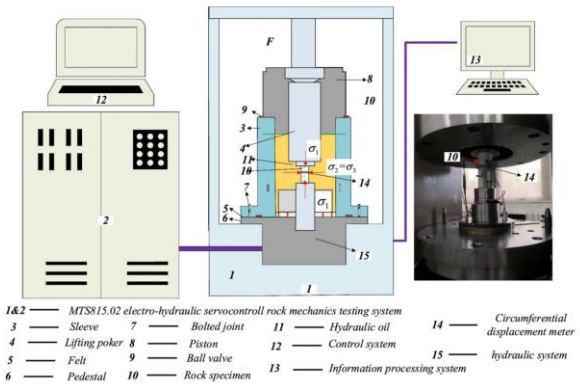

Fig. 1 Schematic of triaxial rock compression tests equipment (Wu *et al*. 2022)

on the 6 input variables. We improve the CNN model and add mean-variance normalization, regularization and dropout to prevent model overfitting. In order to facilitate the prediction and analysis of the data, the stress and strain of the data set used in the model were expanded by a factor of 1,000. The statistical parameters for the training, validation set and test dataset are provided in Table 2.

2.2.1 Box plot representation

The box plot serves as a visual summary of the statistical characteristics of the dataset. Statistical analyses were performed on key parameters such as maximum and minimum values, variance, mean, and quartiles to investigate the influence of rock properties, comprising 6 input variables and strain, as depicted in Fig. 2.

For the case of cyclic loading machine learning models, a dataset with a more comprehensive range is adopted. The number of cycles ranges from 1 to 32, which includes the number of cycles of loading and unloading experienced by most rocks during the experiment. In addition, the mass, density, Young's modulus, confining pressure and stress range from 480.850 g to 877.190 g, 1.95 g/cm^3 to 2.690 g/cm^3, 0.3 MPa to 94.41 MPa , 0 MPa to 60 MPa,0 MPa to 391.985 MPa respectively. The value of strain ranges from 1.73E-05 to 56.41. The maximum strain is more than three million times that of the minimum ones.

2.2.2 Pearson correlation

It's necessary to conduct sensitive analysis on input feature parameters. Due to the complexity and interdependence among different variables, it is not feasible to study the relationship between any single factor and others separately. Pearson correlation coefficient is employed to quantify the linear correlation between two features, with a range of -1 to 1. A coefficient of 1 indicates a perfect positive correlation, -1 signifies a perfect negative correlation, and 0 implies no linear correlation. The corresponding calculation formula is shown in the Eq. (1).

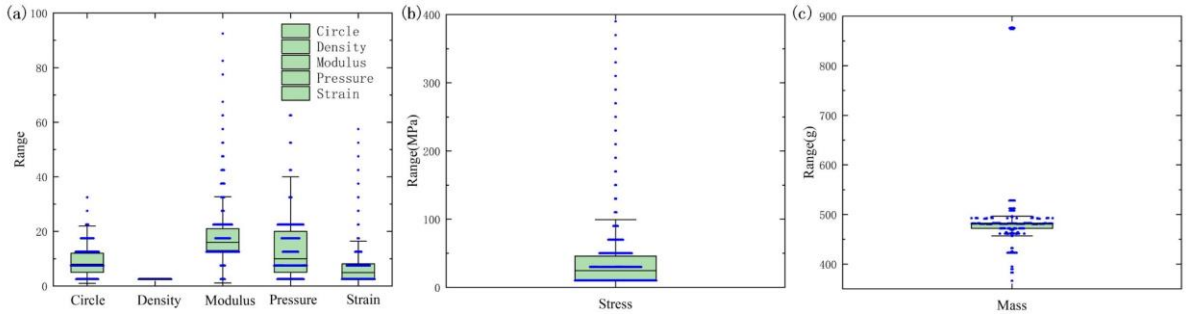

Fig. 2 Box plot for statistical analysis. (a) Circle, Density, Modulus, Pressure, Strain, (b) Stress and (c) Mass

$$Pcc = \frac{\sum_{i=1}^{n}(x_i - \bar{x})(y_i - \bar{y})}{\sum_{i=1}^{n}(x_i - \bar{x})^2 \sum_{i=1}^{n}(y_i - \bar{y})^2} \quad (1)$$

In the equation, Pcc represents the Pearson correlation coefficient, x_i and y_i denote the experimental values of the first and second variables, respectively, and symbolize the average values of the two variables.

Fig. 3 shows the Pearson correlation within 6 input variables and axial strain. For axial strain ε_1, the Pcc values of 0.4565 and 0.4053 between ε_1 and N, M indicate a moderate positive correlation, and the Pcc values of 0.2836 and 0.3318 between ε_1 and σ_3, σ_1 indicate weak correlations. Notably, there exists no linear correlation between ρ, E, and ε_1. Considering the complexity of the experimental data due to multiple types of rocks and confining pressures, traditional regression methods encounter limitations when solving complex nonlinear problems. In contrast, machine learning methods possess distinct advantages in addressing such nonlinear problems.

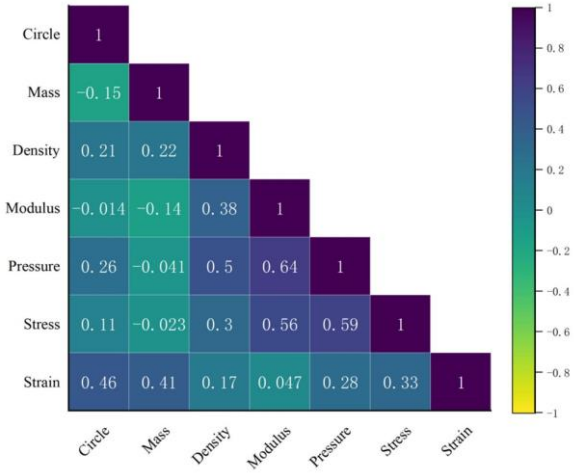

Fig. 3 Pearson correlation within 6 input variables and rock axial strain

2.2.3 Model performance assessment

This study utilizes five statistical indicators to assess the performance of three ML models. As shown in Eqs. (2)-(6). The indicators are coefficient of determination (R^2), mean absolute percentage error (MAPE), root mean square error (RMSE), mean absolute error (MAE) and mean squared error (MSE). The mathematical expressions for the five performance indices are provided below.

$$R^2 = 1 = \frac{\sum_{i=1}^{n}(y_t - y_{pre})^2}{\sum_{i=1}^{n}(y_t - \bar{y})^2} \quad (2)$$

$$MAPE = \frac{100\%}{n} \times \sum_{i=1}^{n}\left|\frac{y_t - y_{pre}}{y_t}\right| \quad (3)$$

$$RMSE \sqrt{\frac{1}{n}\sum_{i=1}^{n}(y_{pre} - y_t)^2} \quad (4)$$

$$MAE = \frac{1}{n}\sum_{i=1}^{n}\left|y_{pre} - y_t\right| \quad (5)$$

$$MSE = \frac{1}{n}\sum_{i=1}^{n}\left|y_t - y_{pre}\right|^2 \quad (6)$$

where n represents the number of data points, y_t and y_{pre} are measured and predicted values.

2.3 Machine learning methods

The back propagation neural network (BPNN) is a widely used ANN model, known for its ability to tackle computationally challenging problems in artificial neural networks such as large-scale data analysis or training. BPNN adopts a three-layer architecture comprising an input layer, a hidden layer, and an output layer. Each layer is processed by processing elements (Basheer and Hajmeer 2000). Each neuron is connected to all neurons in the

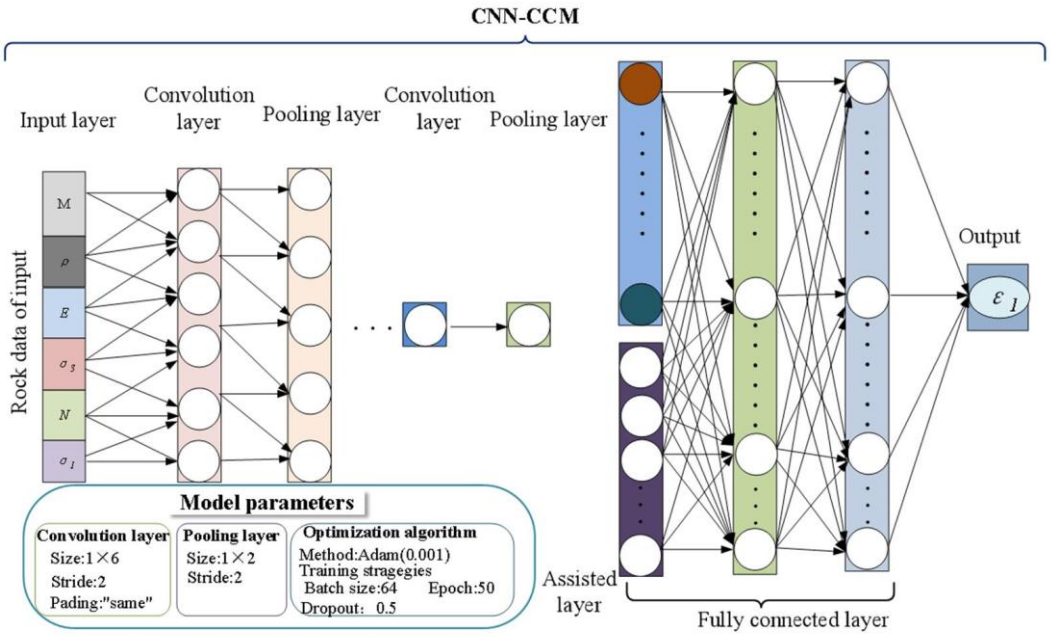

Fig. 4 The structure of CNN-CCM

subsequent layer, and the connecting media is referred to as weights (Zhang *et al*. 2020). Although BPNN is popular in ANN, it has limitations in optimizing weights and thresholds and is susceptible to getting trapped in local optima. The input data flows from the input layer to the output layer, and the error propagates from the output layer to find a set of weights and biases. This process aims to ensure that the network generates output values consistent with the actual output values (Rumelhart *et al*. 1986).

DNN is an artificial neural network characterized by its self-organizing, adaptive, and automatic learning capabilities. Neural networks are extensions of perceptrons, and DNN can be understood as a neural network with many hidden layers. Multi-layer neural networks and deep neural networks actually denote the same concept, with DNN sometimes referred to as a multi-layer perceptron. As depth increases, DNN have more parameters to learn, which can lead to models that overfit on training data and and underperform on new data. DNN, equipped with multiple hidden layers in practice, exhibits accelerated convergence compared to linear layers in conventional linear models. Deep learning models are essentially multi-perceptrons, where each output of a neuron contains outputs from multiple neurons in the hidden layers. The DNN model can determine activation patterns of neurons in response to different input data, thus obtaining the final output.

CNN, a feed-forward neural network, excels at feature extraction from data with convolutional structures. Fig. 4 shows the architecture of a cyclic loading constitutive model based on CNN. A small black box model that describes multiple factors is constructed to predict axial strain through the training and optimization of the parameters by CNN-CCM. The CNN-CCM consists of three levels: Input layer, Hidden layer, Output layer. For the input layer, pre-processing operations are required for input data in the model. The input data include N, M, ρ, E, σ_3 and σ_1 of rock specimens in the axial and triaxial compression test. The hidden layer contains convolution layer, pooling layer, and fully connected layer. The convolution layer is located behind the input layer and consists of a set of filters with trainable parameters to extract data features through convolution operations. The ReLU activation function finds extensive application in CNN as it enhances nonlinear expression and robustness of features and improves the generalization ability of the model. Its mathematical expressions are shown in Eq. (7). The pooling layer is mainly used to reduce the feature dimensionality of the data to prevent over-fitting and improve the fault tolerance of the model. The function of the fully connected layer is to combine the extracted features nonlinearly. The output of ε_1 based on the completion of all layers in the CNN-CCM, and all samples are repeated as above.

$$\mathrm{Re}LU(x)=\begin{cases} x\ if\ x>0 \\ 0\ if\ x\le 0 \end{cases} \tag{7}$$

2.4 CNN-CCM Training

The training process for the improved CNN-CCM is as follows and the process of CNN-CCM is shown in Fig. 5.

(1) Load the necessary packages, import libraries, and build the deep learning model. Construct the CNN model.Input data were normalized for mean-variance at the data preprocessing stage.

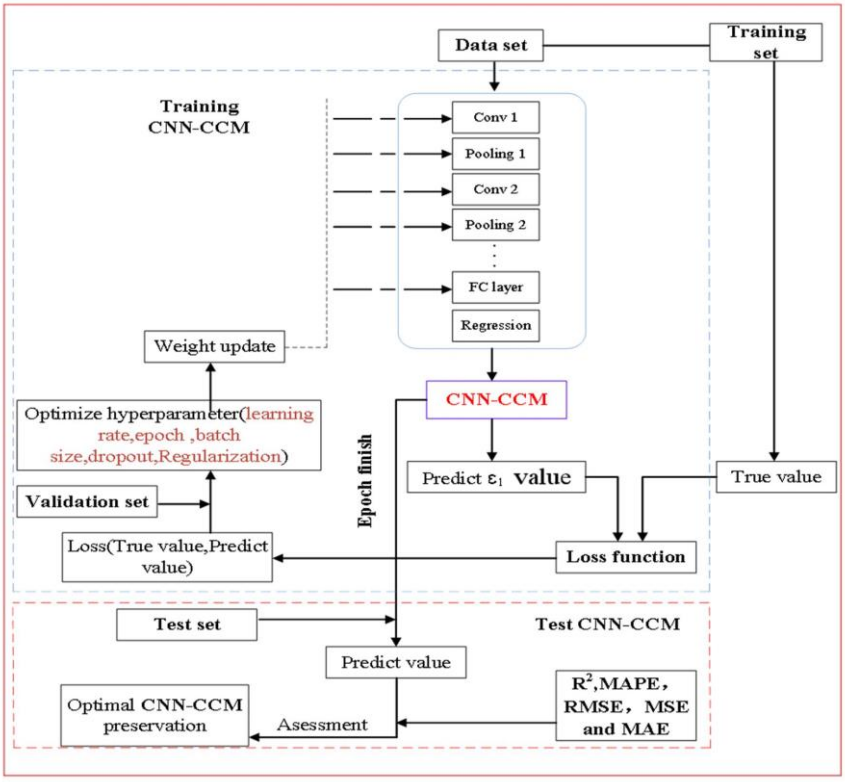

Fig. 5 The process of building CNN-CCM

(2) Load the dataset and use M、 σ_1、 ρ、 N、 σ_3 and E as input features and ε_1 as the output feature. A multifactor single-output analysis was performed. Improve the model and add regularization and dropout to prevent model

overfitting. The model optimization can be achieved through optimization algorithms or adjusting hyperparamet-

ers.The optimal hyperparameters for CNN-CCM are learning rate=0.001, batch-size=64, epoch=50, the number of convolutional layers=5, activation function= ReLU, optimizer= Adam, Dropout =0.5.

(3) Train the deep learning model. In essence, a convolutional neural network functions as a mapping from inputs to outputs. It can learn a vast number of mappings between inputs and outputs without necessitating any precise mathematical expression between the two. When trained on established patterns, a CNN possesses the capability to map between inputs and outputs.

(4) Analyze the results and obtain the optimal model. Through the analysis of the results using evaluation metrics such as R^2, MAPE, and RMSE, MAE, MSE the optimal model can be determined.

3. Results and discussion

3.1 Training results

Table 3 illustrates that the R^2 values for the 13 sets of rock of the CNN-CCM model range from 0.7236 to 0.9781, with 10 sets of data featuring R^2 values of above 0.9, indicating overall good predictive performance of the model. The underperformance of the third sets of rock specimen's prediction can be attributed to the increasing stress with the increase of the loading level, leading to gradual expansion of internal microcracks and higher degrees of damage. This results in significant fluctuations in the stress-strain curve during rock failure. When solely considering the pre-peak stage and disregarding the rock damage stage, the R^2 value is 0.8905. However, evaluating the model exclusively based on R^2 is insufficient. The MAPE of the test set ranges from 8.706% to 27.494%, with 11 sets of data below 20% and 2 sets of data below 30%. These findings affirm the strong applicability of the model. The RMSE varies from 0.0445 to 2.829. Due to the small magnitude of strain in rocks, which makes it inconvenient for data prediction, the strain values of rocks were multiplied by 1000 during the data preprocessing stage. The largest RMSE belongs to the seventh sets of data , which represents marble with a wide range of strain changes, resulting in the largest error. However, the RMSE remains well within a reasonable range. The MSE varies from 0.0020 to 8.3834, the MAE varies from 0.0321 to 2.0132. Overall, accounting for the evaluation criteria of R^2, MAPE, RMSE, MSE and MAE the model demonstrates good generalization performance.

The cyclic loading and unloading constitutive model of rocks is dedicated to describing the stress-strain relationship within each cycle. As a result, accurate prediction within each cycle assume particular significance for the model. Due to space limitations, data from three cycles in the pre-peak stage under four different confining pressures (5 MPa, 15 MPa, 20 MPa, and 40 MPa) were selected for

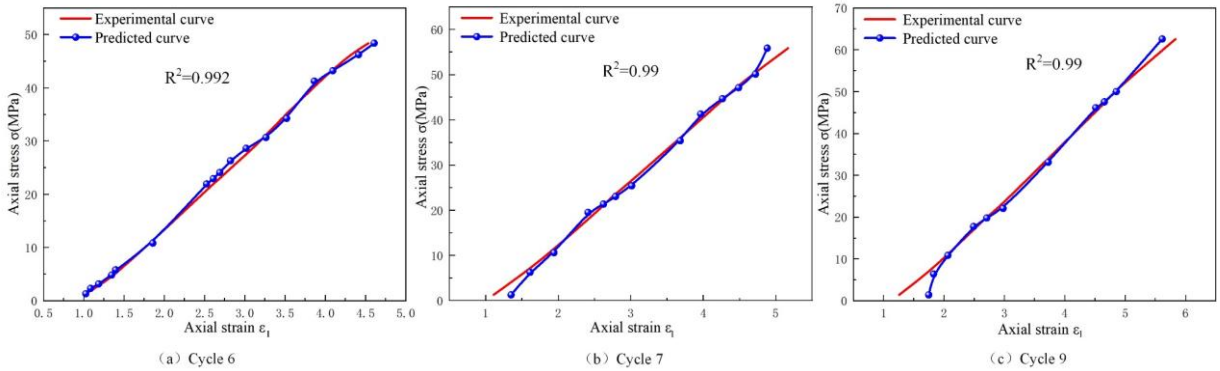

Fig. 6 Predicted data and experimental curve during the loading phase under 5 MPa

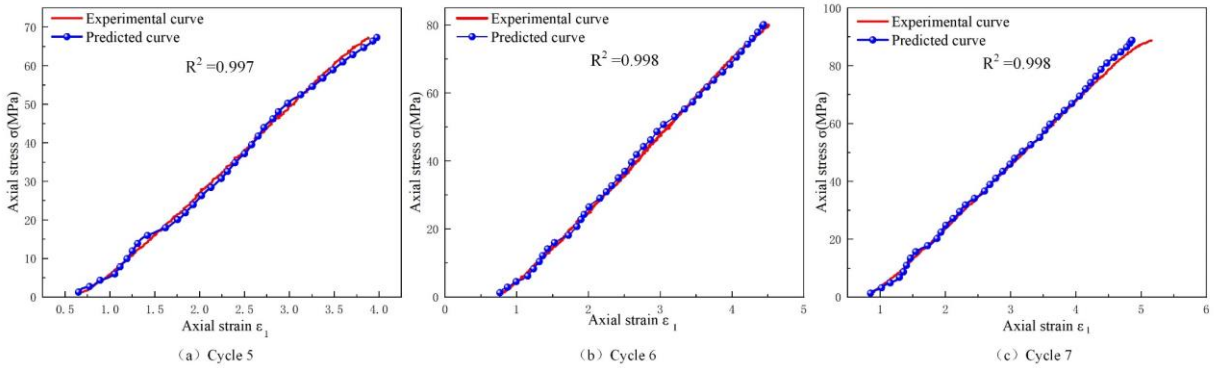

Fig. 7 Predicted data and experimental curve during the loading phase under 15 MPa

Table 3 Evaluation indicators for the 13 sets of data in the test set

Number	R^2	MAPE	RMSE	MSE	MAE
1	0.9101	12.10%	0.2770	0.0767	0.2458
2	0.9533	18.70%	0.6713	0.4507	0.5447
3	0.7236	22.75%	2.8954	8.3834	2.0132
4	0.9154	19.01%	0.7697	0.5924	0.6027
5	0.9557	12.70%	0.5888	0.3467	0.4446
6	0.9417	16.31%	0.9228	0.8515	0.7628
7	0.9090	18.95%	2.8293	8.0052	1.8595
8	0.9358	12.30%	1.2203	1.4891	0.8469
9	0.9727	15.96%	0.8794	0.7733	0.5335
10	0.9781	8.71%	0.4124	0.1701	0.3146
11	0.9725	14.11%	0.0445	0.0020	0.0321
12	0.8155	29.49%	1.2454	1.5511	0.9846
13	0.8497	19.48%	0.4223	0.1783	0.3293

comparison with experimental curves. The results are shown in Figs. 6-9. The stress-strain curves generated by the proposed CNN-CCM constitutive model in this paper exhibit remarkable concordance with the experimental data for each cycle. The proposed model achieves a basic consistency with the stress-strain relationship of the experimental data under different confining pressures and cycle numbers. R^2 values are all above 0.94, indicating a strong correlation between the model and the experimental data.

3.2 Comparative analysis with other Neural Network

To better verify the application of CNN-CCM constitutive models in cyclic loading and unloading, two classic neural networks, namely the Backpropagation Neural Network (BPNN), Deep Neural Network (DNN), were selected for data prediction to compare with CNN-CCM model. Fig. 10 presents the values of R^2, MAPE, RMSE, MSE and MAE obtained from the testing dataset for the three ML-based models. Among the ML-based models, the best performing model on the testing dataset is CNN in terms of the highest R^2 value (0.9289) and lowest MAPE value (16.43%), RMSE value (0.96), MSE value (0.91), MAE value (0.54). BPNN has limitations in optimizing weights and thresholds, and it is easy to fall into a local optimum. DNN has to learn many parameters and is easy to overfit with a long training time. CNN has good advantages in feature extraction.

To provide a more intuitive analysis of the prediction performance, we selected the best 1 rock sample in testing

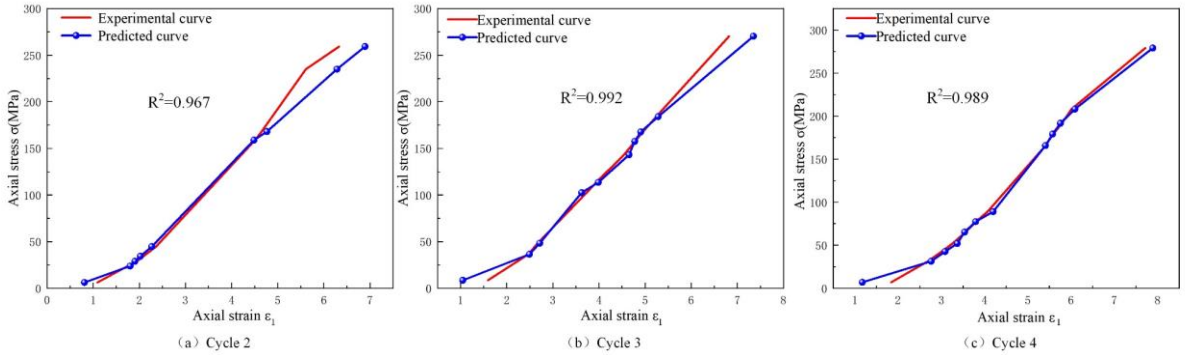

Fig. 8 Predicted data and experimental curve during the loading phase under 20 MPa

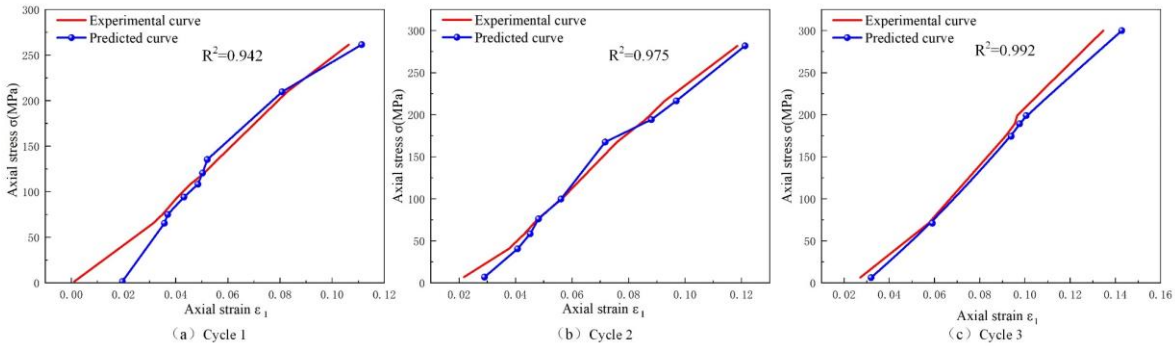

Fig. 9 Predicted data and experimental curve during the loading phase under 40 MPa

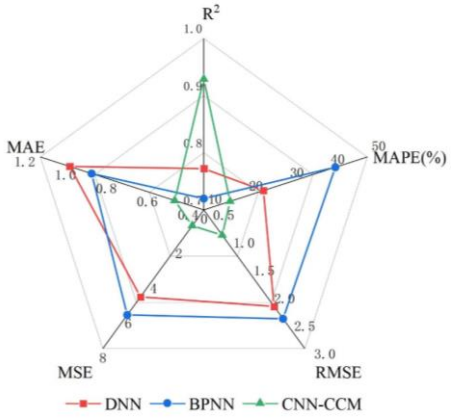

Fig. 10 Radar charts of the three neural networks

dataset from the three neural networks for analysis, as shown in Figs. 11-13. It is evident that the CNN outperforms the other two neural networks in terms of prediction accuracy. It achieves an R^2 value of 0.9781, MAPE of 8.71%, RMSE of 0.4124, MSE of 0.1701, and MAE of 0.3416. It can be observed that the predicted data by CNN are concentrated within a narrower range and closer to the true values.

For the best-performing prediction by the CNN model, which is the 10th sets of data in the test set, the rock specimen undergoes a total of 16 loading and unloading cycles. At the 8th cycle, the sample reaches peak strength, experiences internal structural damage, and undergoes the rapid development of internal fractures, eventually forming intersecting macroscopic fracture surfaces. Cycles 1-7 represent the pre-peak stage, whereas cycles 8-16 denote the damage stage. The stress-strain relationship of the rock during the damage stage is complex and difficult to describe precisely, as shown in Fig. 14. It can be observed that R^2 remains above 0.9 during cycles 1-7, accompanied by MAPE within the 4% to 5% during cycles 4-7, showing minimal differences in RMSE.The largest MSE is 0.07 and the MAE are all below 0.2. From the Analysis of the 8-16 cycles of the failure stage, it becomes evident that R^2 falls below 0.9 remains above 0.77. The RMSE, MAE, MSE of the damage stage were higher than that of the pre-peak stage. indicating poorer prediction than the pre-peak stage. The CNN-CCM constitutive model can accurately fit the test data: the coefficients of determination ranged from 0.79 to 0.99.

3.3 Applicability

To validate the applicability of the CNN-CCM model, three sets of experimental data were extracted from the literature (Gong *et al.* 2022, Liu *et al.* 2016). These data include shale and green sandstone, which exhibit typical brittle characteristics with unstable response after peak stress, alongside poorly cemented and low-strength sandy mudstone characterized by a muddy structure. Although the direct comparison and validation between two models in the

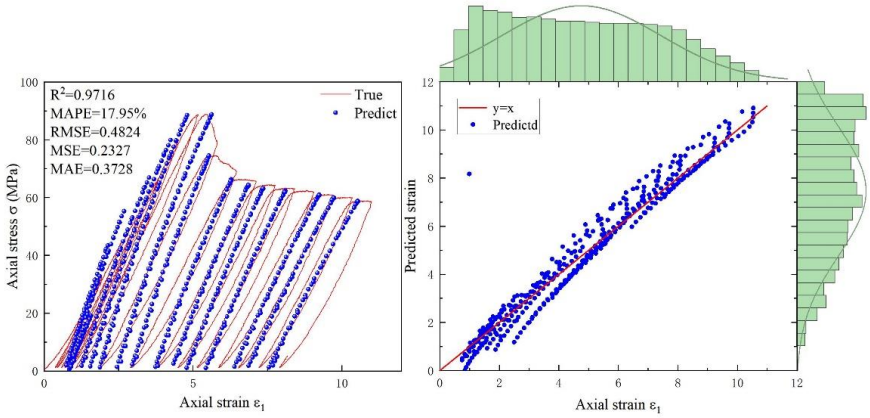

Fig. 11 Prediction results of the BPNN model

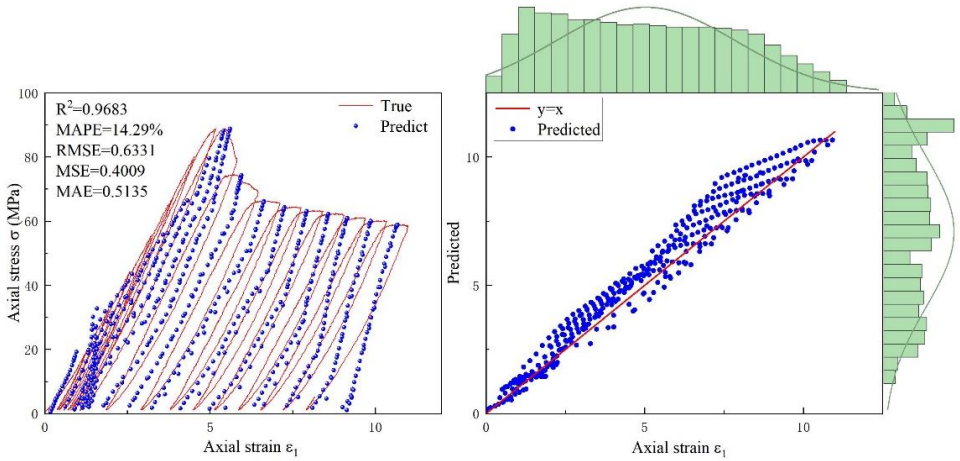

Fig. 12 Prediction results of the DNN model

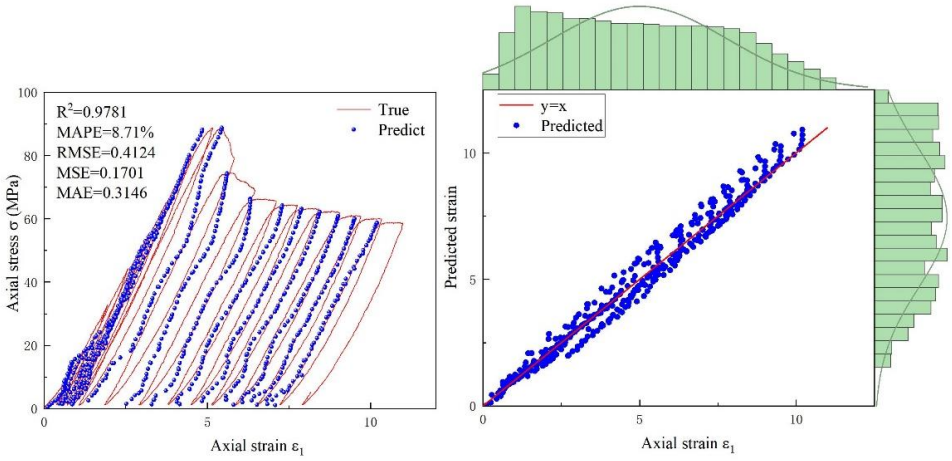

Fig. 13 Prediction results of the CNN model

literature cannot be carried out due to different parameter expressions, meanings, and calculation methods, the proposed model can be used to predict and validate based on different rock experimental curves using the black box model.

Figs. 15-17 show the prediction results of the model for the data not used for training. It can be observed that the R^2 values for both datasets exceed 0.9 and the MAPE values are around 20%. The high deviation in the prediction of the data were poorly cemented sandy mudstones with a pelitic

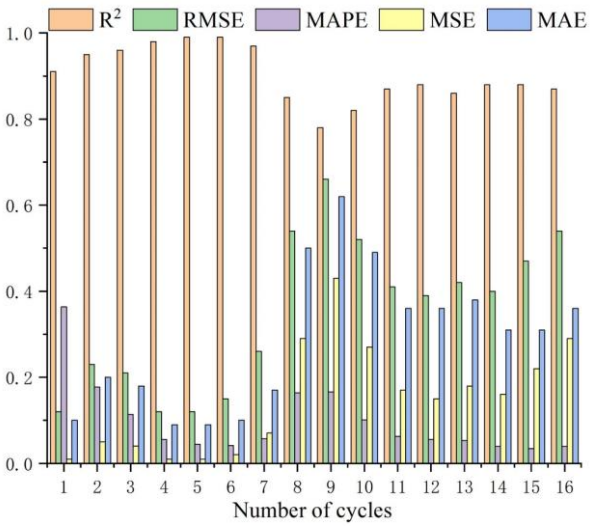

Fig. 14 Single-cycle evaluation index

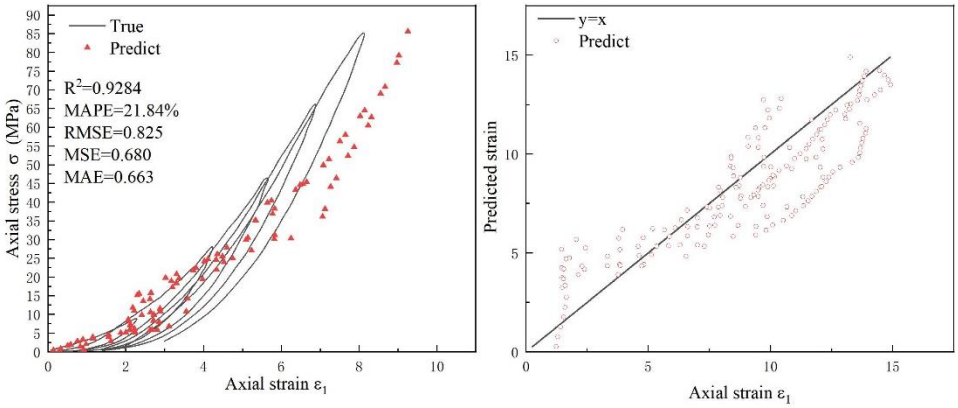

Fig. 15 Overall and distribution scatter plots of shale predictions

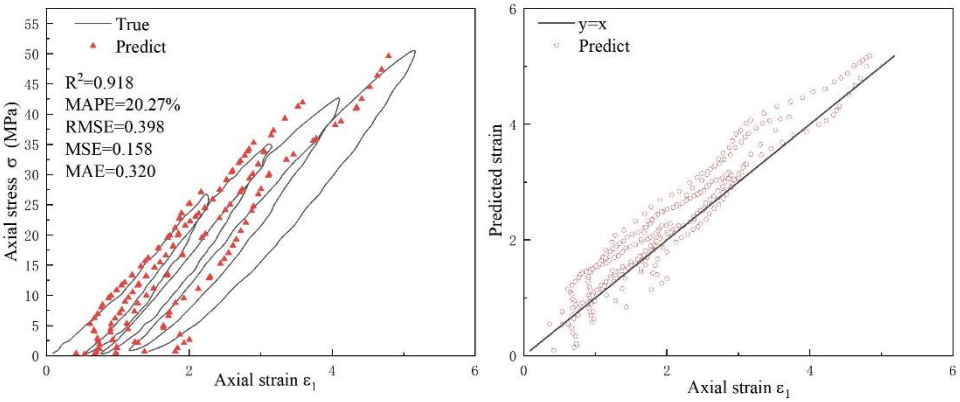

Fig. 16 Overall and distribution scatter plots of sandy mudstone predictions

texture, and a weak strength., as it was sampled from the roof of the No. 20307 coal face, Gaojialiang Mine, Inner Mongolia, China. Although the prediction performance for the three sets of experimental data is not as good as that for the trained data, the model remain demonstrate good generalization ability and suitability for various rocks. Opportunities for improvement persist in future research endeavors.

While the CNN-CCM cyclic constitutive model accurately reflects the constitutive relationship of rocks under graded cyclic loading, further research is needed for the unloading process. Fig. 18 shows the unloading data for the 5th and 6th cycles of the 10th sets of data in the test set. It can be seen that the predicted curve deviates from the experimental curve to some extent and displays lower accuracy than the loading curve.

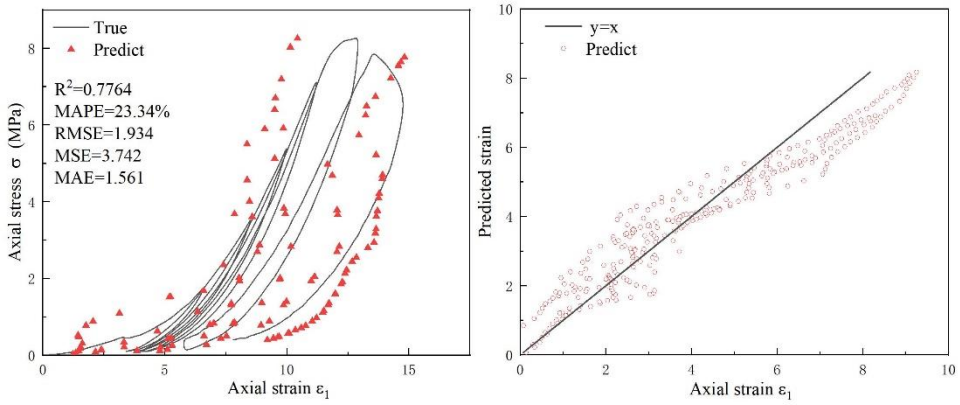

Fig. 17 Overall and distribution scatter plots of green sandstone predictions

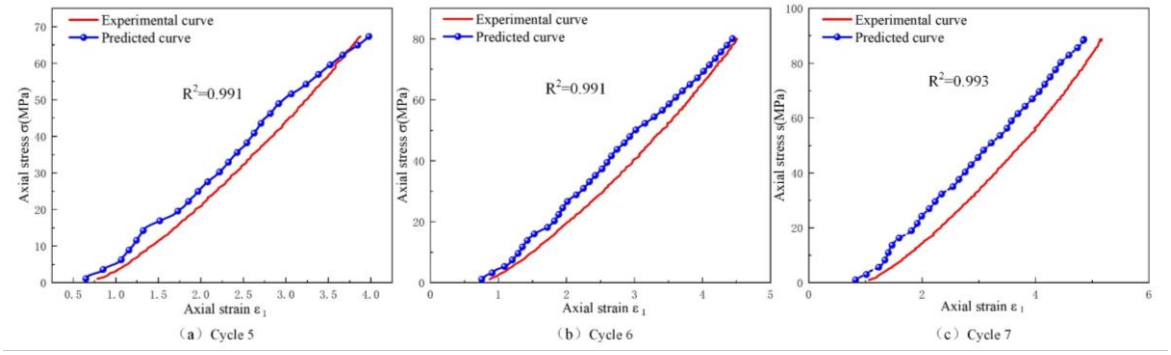

Fig. 18 Comparison of unloading predictions and test curves for 9-th sets of data

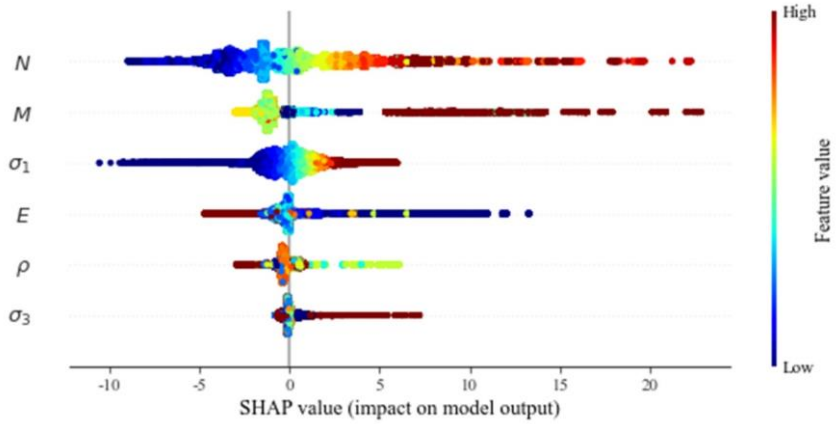

Fig. 19 Summary plot of SHAP

However, the overall trend of the predicted curve is similar to the experimental curve, and the predicted data are all within the hysteresis curve. Overall, the model showcases good generalization ability and suitability. The established model can effectively portrays the hysteresis curve and cyclic loading-unloading characteristics of rocks.

4. SHAP explaining for AI rock constitutive model

Fig. 19 a SHAP summary plot of the 6 features, which demonstrates the distribution of the SHAP values for each feature and indicates the corresponding influences trends,and the color of the dot indicates the value of the specific feature, for which color from blue to red indicates a feature value from low to high.For example, the upper right dot in red means a high mass will lead to a strain prediction increase of around 0.023.Therefore,the summary plot not only offers an understanding of which features are important but also how each feature affects axial strain. Generally, it is observed that with the increase in the cyclic number and mass, the axial strain will increase.

Overall, ρ exerts a negative influence on ε_1, as the rock specimens were made with a standard size of 50 mm×100 mm. Within a certain size range, smaller masses actually have smaller densities.Generally, it is observed that with the

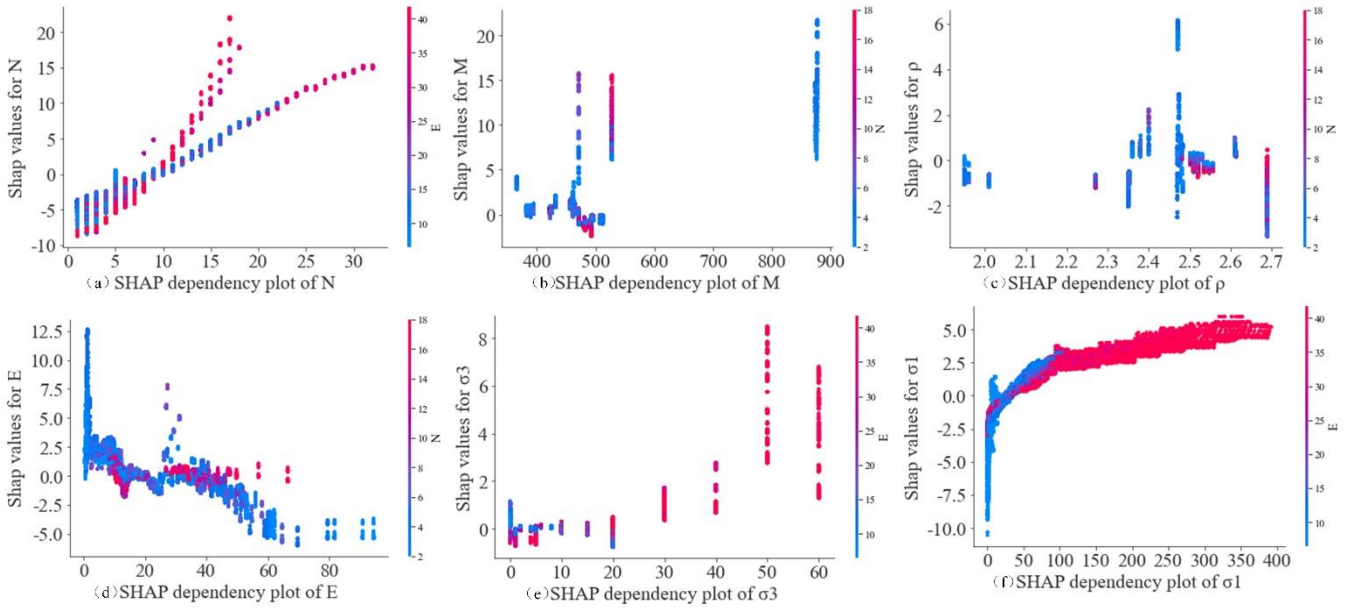

Fig. 20 SHAP Dependency Plot of 6 Input Features

increase in the density, the axial strain will decrease. On the whole, σ_1 has a positive contribution to ε_1 and stands as an important factor affecting ε_1. E has an overall negative effect on ε_1, potentially leading to a reduction in ε as the elastic modulus increases. This is because under cyclic loading and unloading conditions, the elastic modulus of rocks initially increases and subsequently decreases, representing the process of cumulative damage and failure.

It is influenced by the "memory effect" of rocks, where the loading curve of a later level will follow the unloading curve of the previous level. In general, σ_3 also has a positive contribution to ε_1, with a more complex contribution at low values than at higher ones.the axial strain tends to increase with increasing values for confining pressure.This is because the data contains uniaxial compression test data and different types of rocks under the same confining pressure.

This leads to a less obvious contribution at low values.The patterns of positive or negative impact for the six features are consistent with conventional physical equations. However, it's important to note that these six input features are not entirely independent variables; they mutually influence each other. For example, σ_1 is influenced by M, E, and ρ, so the contribution of E may not necessarily be smaller than that of σ_1.

In a Fig. 20 SHAP dependence plot, the feature of interest is plotted on the x-axis, while the SHAP values are plotted on the y-axis. Each data point on the plot corresponds to a specific instance, and its position on the y-axis indicates the impact of the feature value on the model prediction. The color of each data point represents the value of another feature that may be interacting most with the feature of interest.

From Figs. 20(a) and 20(b), it can be seen that N and E have the most interaction. When the number of loading cycles is small, N and E show a positive correlation. However, as the number of loading cycles increases and damage accumulates, N and E become negatively correlated. In general, the trend of N and E is that the elastic modulus of the rock increases first and then decreases with the increase of loading cycles. In Fig. 20(c), when σ_1 is less than 50 MPa, the Shap value < 0, indicating a negative effect on the prediction of axial strain,and when σ_1 exceeds 50MPa, the Shap value > 0,indicating a positive effect on the prediction of axial strain. There is a clear linear relationship between σ_1 and the Shap value between 0 and 400. The distribution pattern of colors also indicates a positive linear relationship between σ_1 and E. Fig. 20(d) shows a positive correlation between σ_3 and the elastic modulus, indicating that the elastic modulus of the rock increases with the increase of confining pressure. As shown in Figs. 20(e) and 20(f), with the change of M and ρ, there is no apparent pattern in the Shap value.By analyzing the SHAP dependence plot, one can infer whether a feature has a positive or negative effect on the model prediction. Additionally, it helps in identifying any non-linear relationships or interactions between different features. It provides a comprehensive view of how different feature values influence the model's output.SHAP dependence plots are particularly useful for interpreting black-box deep learning models,as they provide insights into the model's decision-making process.

5. Conclusions

Compared to traditional cyclic constitutive models, often characterized by numerous parameters without clear meanings and challenging to validate, This study addresses this issue through the application of deep learning theory and laboratory experiments. The main conclusions are as follows:

• The AI Rock Constitutive Model learned by CNN-CCM and 122,152 data. and can predict ε1 using M, σ_1, ρ, N, σ_3,

and *E*. The model's predictive performance was evaluated using 13 different rock samples and 5 evaluation metrics (R^2, *MAPE, RMSE, MSE, MAE*). The R^2 values for the test set data span from 0.7236 to 0.9781, with R^2 above 0.909 for 10 sets of data sets and MAPE ranging from 8.706% to 29.494%. Among them, 11 sets have MAPE below 20%, and RMSE ranges from 0.0445 to 2.829. The MSE varies from 0.0020 to 8.3834,the MAE varies from 0.0321 to 2.0132. The model demonstrates strong generalization capabilities.

• Utilizing the SHAP method for interpreting the AI Rock Constitutive Model reveals a hierarchy of feature importance: $N > M > \sigma_1 > E > \rho > \sigma_3$. Specifically, when the SHAP values for N, M, σ_1, and σ_3 are positive, they positively impact the prediction of strain ε_1; otherwise, they exert a negative influence. In the case of E, a positive value has a negative impact on predicting strain ε_1. This aligns with the typical influence patterns observed in traditional physical rock constitutive equations.

• The limitation of this model lies in its inability to effectively describe the stress-strain relationship during the unloading stage, primarily due to the complexity of cyclic loading and unloading conditions, as well as the restricted variation in rock strains. Further enhancements are required to accurately capture the shape and details of the hysteresis loop.

Declaration of interests

The authors states that they have no known competitive financial interests or personal relationships, which could affect the work reported in this paper.

Data availability statement

Some data, models, or code generated or used during the study (the labeled gold standard for evaluation) are available from the corresponding author by request.

Acknowledgments

All authors contributed to the study conception and design. This work is supported by Henan Natural Science Foundation Youth Fund Project (No.232300421331), Joint fund of the technical R&D program of Henan Province(225200810005),Key Scientific Research Projects of Colleges and Universities in Henan Province (No.23A440005) and Postdoctoral Research Grant in Henan Province (No.202103049), China Postdoctoral Science Foundation (2023M741009).

References

Ahmed, Z., Wang, S., Hashmi, M.Z. Zishan, Z. and Chengjin, Z. (2020), "Causes, characterization, damage models, and constitutive modes for rock damage analysis: a review", *Arabian J. Geosci*., **13**, 806. https://doi.org/10.1007/s12517-020-05755-3.

Ali, U., Muhammad, W., Brahme A, Skiba, O. and Inal, K. (2019), "Application of artificial neural networks in micromechanics for polycrystalline metals", *Int. J. Plasticity*, **120**, 205-219. https://doi.org/10.1016/j.ijplas.2019.05.001.

Basheer, I.A. and Hajmeer, M. (2000), "Artificial neural networks: fundamentals, computing, design, and application", *J. Microbial. Method.*, **43**(1), 3-31.https://doi.org/10.1016/S0167-7012(00)00201-3.

Cerfontaine, B., Charlier, R., Collin F. and Taiebat, M. (2017), "Validation of a new elasto-plastic constitutive model dedicated to the cyclic behaviour of brittle rock materials", *Rock Mech. Rock Eng*., **50**, 2677-2694. https://doi.org/10.1007/s00603-017-1258-3.

Chen, X., Lin, J. Chao, G., Yang, Y., Yin, J.C. and Fan, H. (2021), "Energy evolution characteristics and damage characterization of sandstone under cyclic loading and unloading", *Sci. Technol. Eng*., **22**(14), 5792-5799.

Crotogino, F., Mohmeyer, K.U. and Scharf, R. (2001), Huntorf caes: More than 20 years of successful operation, Orlando, Florida, USA.

Deng, X. (2013), "Study on damage evolution of sandstone and its constitutive model under cyclic loading and unloading", PhD thesis,Jiangxi University of Science and Technology, https://doi.org/10.7666/d.D444605.

Gong, F., Yan, J., Wang, Y. and Luo, S. (2020), "Experimental study on energy evolution and storage performances of rock material under uniaxial cyclic compression", *Shock Vib*., **2020**, https://doi.org/10.1155/2020/8842863.

Gong, F., Zhang, P. and Du, K. (2022), "A novel staged cyclic damage constitutive model for brittle rock based on linear energy dissipation law: modelling and validation", *Rock Mech. Rock Eng*., **55**(10), 6249-6262. https://doi.org/10.1007/s00603-022-02930-8.

Haimson, B. (1978), Effect of cyclic loading on rock, ASTM International, https://doi.org/10.1520/stp35679s.

Heap, M., Faulkner, D., Meredith, P. and Vinciguerra, S. (2010), "Elastic moduli evolution and accompanying stress changes with increasing crack damage: implications for stress changes around fault zones and volcanoes during deformation", *Geophys. J. Int*., **183**(1), 225-236. https://doi.org/10.1111/j.1365-246X.2010.04726.x.

Jiang, D., Chen, J., Ren, S., Xi, Y. and Yang, C. (2013), "A damage constitutive model of rock salt based on acoustic emission characteristics", In: Clean Energy Systems in the Subsurface: Production, Storage and Conversion: Proceedings of the 3rd Sino-German Conference "Underground Storage of CO2 and Energy", Goslar, Germany, 21-23 May 2013. https://doi.org/CNKI:SUN:ZNGD.0.2013-12-037.

Jiang, Q., Liu, X., Li, S., Liu, J., Liu, Q. and Sun, W. (2023), "Coupling deterioration model of mechanical parameters for the jinping marble under progressive damage conditions", *Rock Mech. Rock Eng*., **56** (6), 3993-4018. https://doi.org/10.1007/s00603-023-03268-5.

Jing, L., Li, X., Yan, Y., *et al*. (2022), "Study on the constitutive model of coal rock damage under hierarchical cyclic loading and unloading", *Coal Mine Saf*., **53**(1), 8. https://doi.org/10.13347/j.cnki.mkaq.2022.01.011.

Li, X., Cao, W.G. and Su, Y.H. (2012), "A statistical damage constitutive model for softening behavior of rocks", *Eng. Geol*., **143**, 1-17. https://doi.org/10.1016/j.enggeo.2012.05.005.

Liu, T.W., He, J.D. and Xu, W.J. (2013), "Energy properties of failure of marble samples under triaxial compression", *Chinese J. Geotech. Eng*., **35**(2), 395-400. https://doi.org/CNKI:SUN:YTGC.0.2013-02-027.

Liu, X.M., Li, X., Liu, J. and Zhao, M. (2011), "Slacking

mechanism of red sandstone based on energy dissipation principle", *J. Central South Univ*., (Science and Technology), **42**(10), 3143-3149. https://doi.org/CNKI:SUN:ZNGD.0.2011-10-043.

Liu, X.S., Ning, J., Tan, Y. and Gu, Q. (2016), "Damage constitutive model based on energy dissipation for intact rock subjected to cyclic loading", *Int. J. Rock Mech. Min Sci*., **85**, 27-32. https://doi.org/10.1016/j.ijrmms.2016.03.003.

Liu, Y., Dai, F., Zhao, T. and Xu, N. (2017), "Numerical investigation of the dynamic properties of intermittent jointed rock models subjected to cyclic uniaxial compression", *Rock Mech. Rock Eng*., **50**, 89-112. https://doi.org/10.1007/s00603-016-1085-y.

Liu, Z., Zhao, G., Meng, X., Zhang, R., Chunliang, D. and Xu, W. (2021), "Energy analysis method for uniaxial compression test of sandstone under static and quasi dynamic loading rates", *Adv. Mater. Sci. Eng*., **2021**(6), 1-11. https://doi.org/10.1155/2021/9933243.

Luo, J. and Li, X. (2020), "Constitutive model of rock damage under cyclic loading and unloading", *J. Anhui Univ. Sci. Technol*., (Natural Science Edition), https://doi.org/CNKI:SUN:HLGB.0.2020-01-003.

Meng, Q., Wang, C., Huang, B., *et al* (2020), "Rock energy evolution and distribution law under three-axis cyclic loading and unloading conditions", *Chinese J. Rock Mech. Eng*., **39**(10), 13. https://doi.org/10.13722/j.cnki.jrme.2020.0208.

Mo, H. (1988), "Cyclic experiments of rocks and study of constitutive relationships", *Chinese J. Rock Mech. Eng*., **7**(3), 215-224

Moradian, Z., Einstein, H.H. and Ballivy, G. (2016), "Detection of cracking levels in brittle rocks by parametric analysis of the acoustic emission signals", *Rock Mech. Rock Eng*., **49**, 785-800. https://doi.org/10.1007/s00603-015-0775-1.

Pourhosseini, O. and Shabanimashcool, M. (2014), "Development of an elasto-plastic constitutive model for intact rocks", *Int. J. Rock Mech. Min. Sci*., **66**, 1-12. https://doi.org/10.1016/j.ijrmms.2013.11.010.

Ray, S., Sarkar, M. and Singh, T. (1999), "Effect of cyclic loading and strain rate on the mechanical behaviour of sandstone", *Int. J. Rock Mech. Min. Sci*., **36**(4), 543-549. https://doi.org/10.1016/S0148-9062(99)00016-9.

Rumelhart, D.E., Hinton, G.E. and Williams, R.J. (1986), "Learning representations by back-propagating errors", *Nature*, **323**(6088), 533-536. https://doi.org/10.7551/mitpress/1888.003.0013.

Sloan, J., Filz, G. and Collin, J. (2013), "Field-scale column-supported embankment test facility", *Geotech. Test. J*., **36**(6), 891-902. https://doi.org/10.1520/gtj20120229.

Su, C. and Yang, S. (2006), "Test of rock sample deformation and strength characteristics under cyclic loading and unloading", *J. Hohai Univ*., **34**(6), 5. https://doi.org/10.3321/j.issn:1000-1980.2006.06.016.

Sun, Z.K. (2022), "Study on mechanical properties and energy evolution of sandstone under cyclic loading and unloading", PhD thesis, Shenyang Jianzhu University, https://doi.org/10.27809/d.cnki.gsjgc.2021.000215.

Taheri, A. and Tatsuoka, F. (2013), "A new method to simulate stress–strain relations from multiple-step loading triaxial compression test results", *Geotech. Test. J*., **36**(6), 799-810. https://doi.org/10.1520/gtj20130005.

Tao, Z. and Mo, H. (1990), "An experimental study and analysis of the behaviour of rock under cyclic loading", *Int. J. Rock Mech. Min. Sci. Geomech. Abstracts*, **27**(1), 51-56. https://doi.org/10.1016/0148-9062(90)90008-P.

Tian, Y. and Yu, R. (2014), "Energy analysis of limestone during triaxial compression under different confining pressures", *Rock Soil Mech*., **35**(1), 118-129. https://doi.org/CNKI:SUN:YTLX.0.2014-01-018.

Wang, C. (2022), "Study on the damage evolution law of red sandstone under different cyclic loading and unloading paths", https://doi.org/10.27860/d.cnki.gsxwl.2021.000050.

Wang, Z., Li, S., Qiao, L. and Zhao, J. (2013), "Fatigue behavior of granite subjected to cyclic loading under triaxial compression condition", *Rock Mech. Rock Eng*., **46**, 1603-1615. https://doi.org/10.1007/s00603-013-0387-6.

Wang, Z.C., Zhao, J., Li, S., *et al.* (2012), "Fatigue mechanical properties of granite under cyclic loading and its constitutive model", *Chinese J. Rock Mech. Eng*., **31**(9), 1888-1900. https://doi.org/10.3969/j.issn.1000-6915.2012.09.021.

Wu, L.Y., Ma, D., Wang, Z., Zhang, J., Zhang, B., Li, J., Liao, J. and Tong, J. (2023), "A deep cnn-based constitutive model for describing of statics characteristics of rock materials", *Eng. Fract. Mech*., **279**. https://doi.org/10.1016/j.engfracmech.2023.109054.

Wu, L.Y., Wang, Z., Ma, D., Zhang, J., Wu, G., Wen, S., Zha, M. and Wu, L. (2022), "A continuous damage statistical constitutive model for sandstone and mudstone based on triaxial compression tests", *Rock Mech. Rock Eng*., **55**(8), 4963-4978. https://doi.org/10.1007/s00603-022-02924-6.

Wu, S., Zhao, S., Wu, D. and Wang, Y. (2018), "Constitutive modelling for restrained recovery of shape memory alloys based on artificial neural network", *Neuro Quantology*, **16**(5). https://doi.org/10.14704/nq.2018.16.5.1387.

Xiao, J.Q., Ding, D.X., Jiang, F.L. and Xu, G. (2010), "Fatigue damage variable and evolution of rock subjected to cyclic loading", *Int. J. Rock Mech. Min. Sci*., **47**(3), 461-468. https://doi.org/10.1016/j.ijrmms.2009.11.003.

Xie, H., Ju, Y., Li, L., *et al.* (2008), "The energy mechanism of the deformation and failure process of rock mass", *Chinese J. Rock Mech. Eng*., **27**(9), 1729-1740. https://doi.org/10.3321/j.issn:1000-6915.2008.09.001.

Xie, H.P. (1990), Rock concrete damage mechanics, Rock concrete damage mechanics

Xu, L., Yang, Y., Zhang, Y., Xue, Y., Yu, Y. and Hao, N. (2023), "Estimation of stress–strain constitutive model for ultra-high performance concrete after high temperature with an deep neural network based method", *Constr. Build. Mater*., **408**, 133690. https://doi.org/10.1016/j.conbuildmat.2023.133690.

Xu, W. and Wei, L. (2002), "Study of statistical constitutive model of rock damage", *Chinese J. Rock Mech. Eng*., **21**(6), 787-791. https://doi.org/10.3321/j.issn:1000-6915.2002.06.006.

Yang, D.F., Zhang, D., Niu, S., Dang, Y., Feng, W. and Ge, S. (2018), "Experiment and study on mechanical property of sandstone post-peak under the cyclic loading and unloading", *Geotech. Geol. Eng*., **36**, 1609-1620. https://doi.org/10.1007/s10706-017-0414-6.

Zhang, J., Yin, Y., Shi, W., Bian, H., Shi, L., Wu, L., Han, Z., Zheng, J., He, X. (2023), "Strength and uniformity of EICP-treated sand under multi-factor coupling effects", *Biogeotechnics*. **1**(1), 100007. https://doi.org/10.1016/j.bgtech.2023.100007.

Zhang, M. (2019), "Study on infrasonic characteristics and damage characterization of red sandstone under cyclic loading and unloading", PhD thesis, Jiangxi University of Science and Technology. https://doi.org/CNKI:CDMD:2.1018.065200.

Zhang, P.Y., Xia, C.C., Zhou, S.W., *et al.* (2015), "Study on cyclic addition unloading rock constitutive model", *Geomechanics*, **36**(12), 3354-3359. https://doi.org/10.16285/j.rsm.2015.12.002.

Zhang, R., Liu, Y. and Sun, H. (2020), "Physics informed multi-lstm networks for metamodeling of nonlinear structures", *Comput. Method. Appl. M*., **369**, 113226. https://doi.org/10.1016/j.cma.2020.113226.

Zhou, J.T. (2019), "Experimental study on acoustic emission characteristics of rock materials with different particle sizes

under cyclic loading and unloading conditions", PhD thesis, Jiangxi University of Science and Technology.

Zhou, L. (2018), "Experiment research on the deformation characteristics and damage variable expression of marble under cyclic load", PhD thesis, Huaqiao University. https://doi.org/CNKI:CDMD:2.1018.887007.

Zhou, S.W., Xia, C.C., Zhao, H.B., Mei, S.H. and Zhou, Y. (2017), "Statistical damage constitutive model for rocks subjected to cyclic stress and cyclic temperature", *Acta Geophysica*, **65**, 893-906. https://doi.org/10.1007/s11600-017-0073-2.

Zhou, T.B., Qin, Y., Ma, Q. and Liu, J. (2019), "A constitutive model for rock based on energy dissipation and transformation principles", *Arabian J. Geosci*., **12**, 1-14. https://doi.org/10.1007/s12517-019-4678-4.

GC